Eur. Phys. J. B **17**, 615–622 (2000)

**THE EUROPEAN PHYSICAL JOURNAL B**

EDP Sciences


# Study of the ferrodistorsive orbital ordering in $NaNiO_2$ by neutron diffraction and submillimeter wave ESR

E. Chappel[1,a], M.D. Núñez-Regueiro[1], G. Chouteau[1], O. Isnard[2], and C. Darie[2]

[1] Grenoble High Magnetic Field Laboratory, CNRS and MPI-FKF, BP 166X, 38042 Grenoble, France
[2] Laboratoire de Cristallographie, CNRS, BP 166X, 38042 Grenoble, France

Received 29 May 2000

**Abstract.** $NaNiO_2$ has been studied by neutron-powder diffraction, magnetic susceptibility and submillimeter wave ESR. The monoclinic structure at room temperature is characterised by a ferrodistorsive orbital ordering due to the Jahn-Teller (JT) effect of the $Ni^{3+}$ ions in the low spin state. $NaNiO_2$ undergoes a structural transition at around 480 K, above which the orbital ordering disappears. The high temperature phase is rhombohedral with the layered $\alpha$–$NaFeO_2$ structure ($R\bar{3}m$ space group). The magnetic susceptibility exhibits hysteresis and we observe a change of the Curie-Weiss law parameters above the JT transition. The anisotropy of the $g$-factor at 200 K can be attributed to the JT effect which favours the $\mid 3z^2 - r^2\rangle$ orbital occupation. Finally, the interplay between the magnetic and structural properties of $NaNiO_2$ and $Li_{1-x}Ni_{1+x}O_2$ is discussed.

**PACS.** 71.70.Ej Spin orbit coupling, Zeeman and Stark splitting, Jahn-Teller effect – 61.12.-q Neutron diffraction and scattering – 76.30.-v Electron paramagnetic resonance and relaxation

## 1 Introduction

The $AMO_2$ oxides (with A = H, Ni, Na and M = 3$d$-metal) are promising materials for battery applications. A and M hexagonal layers alternate in these compounds. The O ions connect the M ions both within the same layer and between adjacent layers giving rise to ferromagnetic or antiferromagnetic interactions, depending on the bond angle. Among these compounds, $Li_{1-x}Ni_{1+x}O_2$ is the subject of strong theoretical interest due to the possible coupling between spin and orbital degrees of freedom.

In fact, the absence of a cooperative Jahn-Teller effect (CJTE) and of spin ordering in this system has been recently interpreted as the realisation of an orbital-spin liquid state. Quantum fluctuations between degenerate classical configurations [1] or simply the frustration of the triangular $Ni^{3+}$ lattice [2] are invoked as reasons preventing any long range ordering. On the other hand, the particular magnetic properties of this compound, which is never stoichiometric, have been attributed to the competition between the interactions induced by the excess Ni ions in the Li layers, with the magnetic interactions analogous to those present in $NaNiO_2$ [3]. The parent compound $NaNiO_2$ is an A-type antiferromagnetic insulator with a ferrodistorsive orbital ordering due to the CJTE breaking of the orbital degeneracy of the $Ni^{3+}$ ions with $(t_{2g}^6 e_g^1)$ configuration. This system was synthesised for the first time by Dyer *et al.* in 1954 [4]. The magnetic structure was derived from magnetization measurements on a single crystal by Bongers and Enz in 1966 [5]. The structure of the low temperature monoclinic phase has been determined by Dick *et al.* [6], while Delmas *et al.* [7] have studied the effect of the Co substitution on the JT distortion.

Chappel *et al.* [8] have performed a complete static and dynamical magnetic study at low temperatures. However, to our knowledge, besides these references no other works exist devoted to this compound. Therefore, the detailed analysis of the development of the CJTE and improved data, both, above and below the transition in $NaNiO_2$, are desirable in order to understand the interplay between the magnetic and structural properties in this family of compounds.

## 2 Experimental

Powder samples of $NaNiO_2$ were prepared by reaction of 3.5 g of NiO and 2.62 g of $Na_2O_2$ in an $Al_2O_3$ crucible. Intimately ground mixture was heated under pure dry oxygen for 70 h at temperature of 700 °C, and then allowed to cool slowly to room temperature still under oxygen atmosphere. The resulting powder was a mixture of $NaNiO_2$ with a small amount of NiO. Refiring this mixture with an excess of $Na_2O_2$ (0.5 g) during 3 days with intermediate grinding led to pure samples of $NaNiO_2$.

X-ray powder patterns were collected for $10° \leq 2\theta \leq 90°$ with a Siemens D5000 powder diffractometer in

[a] e-mail: chappel@labs.polycnrs-gre.fr

**Table 1.** Structural and reliability factors (%) of $NaNiO_2$ below and above the JT transition. The numbers in parentheses are the statistical errors of the last significant digits.

| | $a$ (Å) | $b$ (Å) | $c$ (Å) | $\beta$ (°) | $R_p$ | $R_{\rm wp}$ | $R_{\rm exp}$ | $R_{\rm Bragg}$ | $\chi^2$ |
|---|---|---|---|---|---|---|---|---|---|
| room T ($C2/m$) | 5.311(1) | 2.840(1) | 5.568(1) | 110.44(1) | 3.07 | 3.89 | 0.74 | 3.00 | 27.5 |
| 565 K ($R\bar{3}m$) | 2.9602(2) | 2.9602(2) | 15.759(4) | | 3.14 | 4.18 | 1.29 | 2.46 | 10.5 |

transmission mode, equipped with a Ge monochromator placed on the primary beam ($CuK_{\alpha_1}$ radiation, $\lambda$ = 1.54056 Å), a rotating sample and a mini PSD.

Neutron diffraction experiments were done at the Institut Laue-Langevin reactor using the high flux D1B instrument (CRG-CNRS) operating at 2.52 Å neutrons and a position sensitive detector that simultaneously collects data over a range of 80° in $2\theta$. The neutron diffraction patterns were recorded at different temperatures between 2 and 300 K in a dedicated cryostat. The high temperature analysis of the structural phase transformation has been performed between room temperature and 600 K in a furnace. In order to avoid diffraction from the sample holder and/or the furnace, both were made of vanadium. The structure analysis has been undertaken with the Rietveld method implemented with the Fullprof program [9].

X-band EPR measurements were carried out at 9.44 GHz in the temperature range 5–300 K using a Bruker spectrometer. Special care was taken to keep constant the $Q$-factor of the resonant cavity.

Submillimeter wave electron spin resonance (ESR) measurements were carried out between 25 and 300 K in the frequency range 95–285 GHz using Gunn oscillators. The magnetic field (up to 12 tesla) is produced by a superconducting magnet.

Magnetic susceptibility measurements were performed on an extraction magnetometer at 1 T between 300 and 600 K using pressed pellets.

## 3 Results

### 3.1 Neutron diffraction

The thermal analysis of the diffraction patterns presented in Figure 1 shows the phase transition of $NaNiO_2$. One can clearly see that the structural change is shifted in temperature by heating or cooling, respectively. It takes place between 480 and 500 K when the samples are heated but between 465 and 445 K when they are cooled.

The high temperature phase is rhombohedral with the layered $\alpha$–$NaFeO_2$ structure ($R\bar{3}m$ space group), which can also be described from a packing of Na and $NiO_2$ slabs built up of edge sharing $NiO_6$ octahedra to form a triangular Ni lattice. In Figure 2 we present the observed and calculated diffraction patterns of $NaNiO_2$, both below and above the structural transition. Traces of $Na_2Ca_3$ impurity have been found and they are indicated as the second row of ticks in Figure 2. The refinement leads to an estimation of the impurity content lower than 4%.

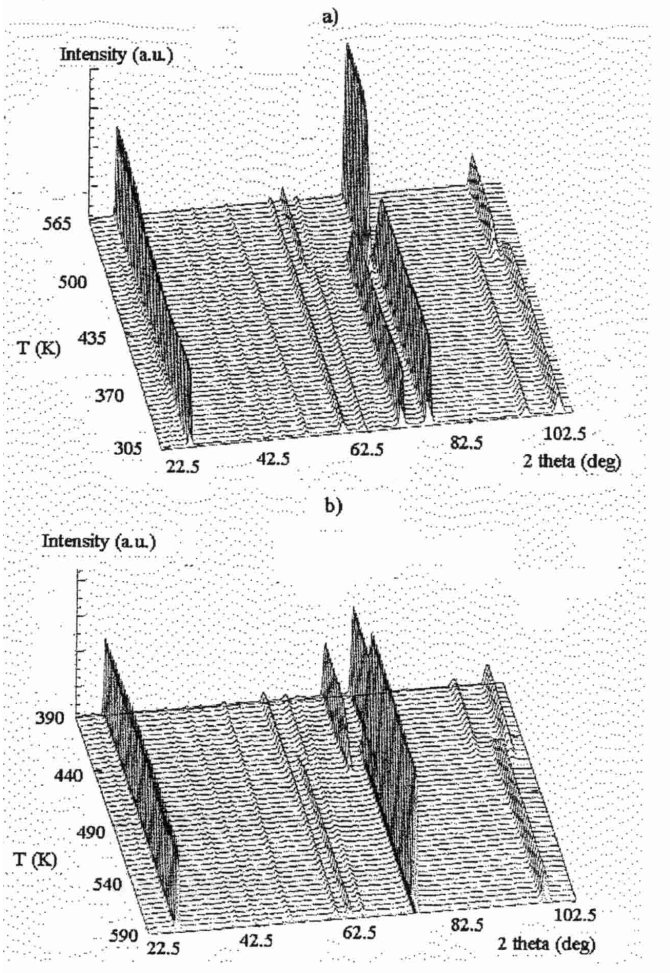


**Fig. 1.** Temperature dependence of neutron powder diffraction patterns of $NaNiO_2$ obtained (a) on heating, (b) on cooling.

Tables 1, 2 and 3 summarise the geometrical parameters that are directly related to the JT effect.

The lift of the degeneracy of the $e_g$ orbitals due to the JT effect can be described by the distortion of the $NiO_6$ octahedra. The $NaNiO_2$ low temperature phase is monoclinic, space group $C2/m$, which can be derived from the rhombohedral high temperature structure: the oxygen ions form a distorted hexagonal close-packed arrangement. The $NiO_6$ (and $NaO_6$) octahedra are distorted (elongated)

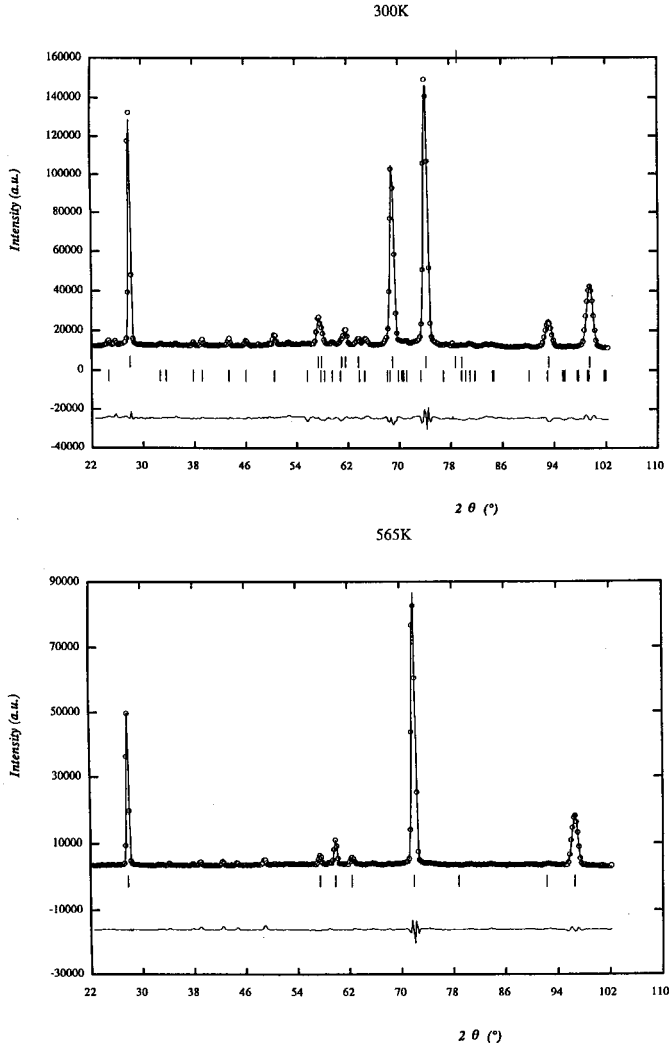


**Fig. 2.** Observed and calculated neutron diffraction patterns (the lowest curve indicates their difference) of $NaNiO_2$ below and above the JT transition. The first and second row of ticks refer to the nuclear contribution of $NaNiO_2$ and $Na_2Ca_3$ respectively, to the diffraction pattern.

with 4 short (gray) and 2 long (black bonds in Fig. 3) Ni-O distances of 1.91 and 2.14 Å, respectively. This distortion is characteristic of JT ions like the low spin state of $Ni^{3+}$ with $(t_{2g}^6 e_g^1)$ configuration. All octahedra undergo the same elongation and a macroscopic distortion is observed: this state is referred as ferrodistorsive orbital ordering.

The temperature dependence of the lattice parameters when the samples are heated is shown in Figure 4. We observe a linear regime below and above the JT transition. Fitting the spectra with only one structure when approaching the transition becomes difficult, and we observe a strong increase of the error bars. Between 480 and 500 K the two phases are simultaneously present. Between 2 and 300 K the cell parameters do not change much ($a$ = 5.339(4) Å, $b$ = 2.860(2) Å, $c$ = 5.599(6) Å, and $\beta$ = 110.43(6)° at 1.6 K), and they are similar to

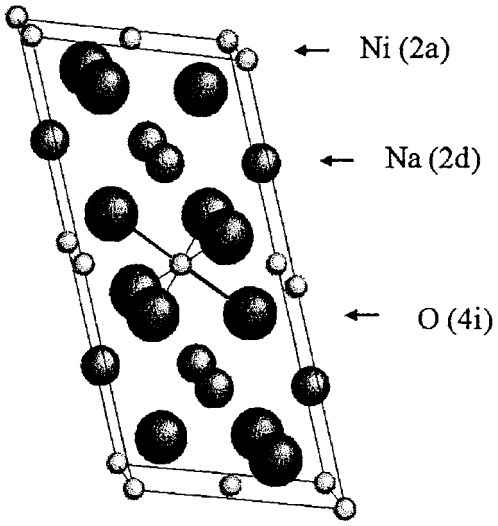


**Fig. 3.** Sketch of the $C_m^2$ layered structure of $NaNiO_2$ showing the deformation of the $NiO_6$ octahedron, with 2 long (black) and 4 short (gray) bond lengths, responsible for the $R\bar{3}m \rightarrow C_m^2$ crystallographic transition.

**Table 2.** Refined atomic positions and average Debye-Waller factors B of the low and high temperature phases of $NaNiO_2$.

| | atom | site | $x$ | $y$ | $z$ | $B$ |
|---|---|---|---|---|---|---|
| room T | Na | 2d | 0 | 0.5 | 0.5 | 0 |
| ($C_m^2$) | Ni | 2a | 0 | 0 | 0 | 0.2(7) |
| | O | 4i | 0.2832(4) | 0 | 0.804(7) | 0.8(5) |
| 565 K | Na | 3a | 0 | 0 | 0 | 0.9(5) |
| ($R\bar{3}m$) | Ni | 3b | 0 | 0 | 0.5 | 0.2(5) |
| | O | 6c | 0 | 0 | 0.230(8) | 1.4(2) |

**Table 3.** Interatomic distances and angles of $NaNiO_2$ at the low and high temperature phases.

| | room T | 565 K |
|---|---|---|
| Ni-O Å | 1.91 (×4)<br>2.14 (×2) | 1.98 (×6) |
| Ni-Ni(layer) Å | 2.84 (×2)<br>3.01 (×4) | 2.96 (×6) |
| $\theta$ = Ni-O-Ni(layer)(°) | 95.67 (×4)<br>95.90 (×2) | 96.43 (×6) |

those observed in the low temperature phase study by Dick *et al.* [6].

### 3.2 Magnetic susceptibility

In Figure 5 we report the temperature dependence of $H/M$ for $NaNiO_2$. The open and filled circles correspond to measurements on cooling and heating, respectively. The points can be fitted with a Curie-Weiss law between 300 and 450 K, with an effective moment $\mu_{\text{eff}} = 1.85\mu_B$ and a Weiss temperature of $\theta = +36$ K. The hysteresis observed around 480 K is due to the JT transition from the monoclinic to the trigonal symmetry. Above the JT transition

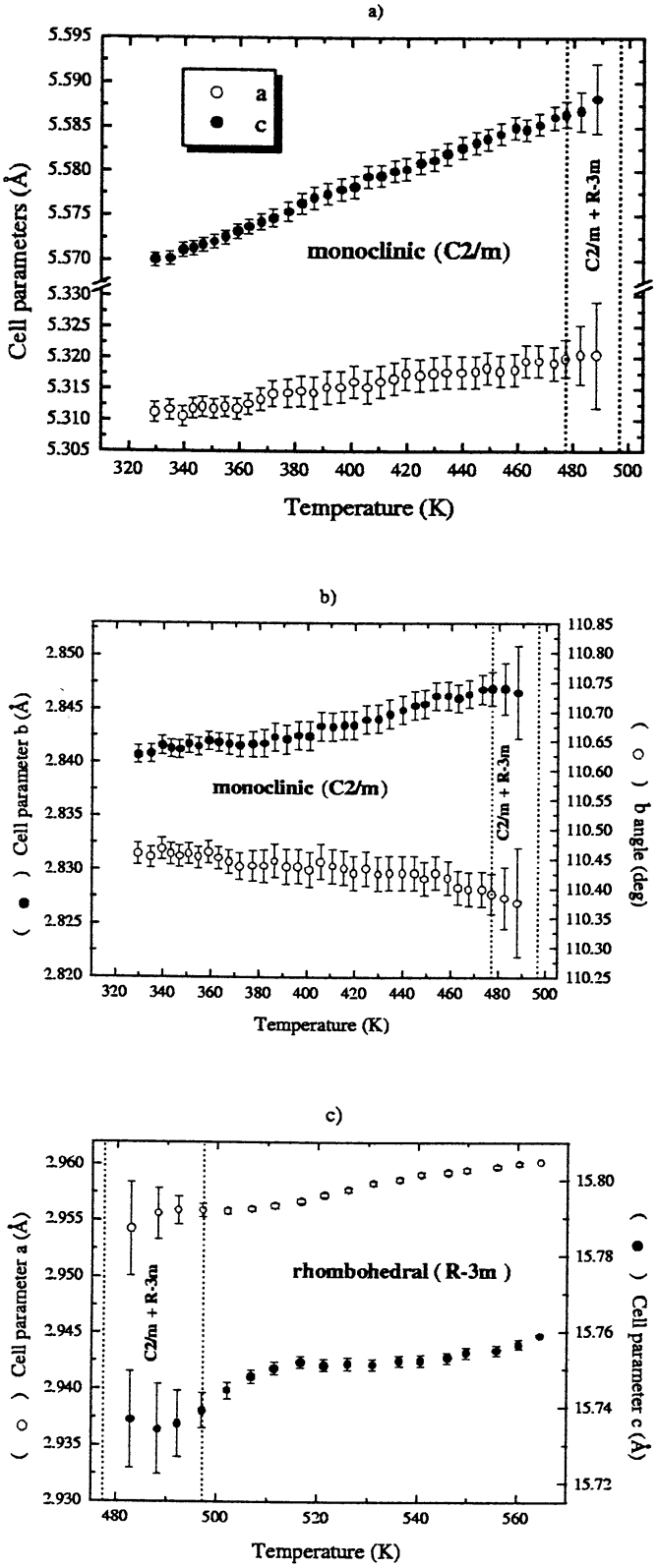


**Fig. 4.** Cell parameters of $NaNiO_2$ as a function of temperature obtained by heating: a) a and c; b) b and $\beta$ parameters of the monoclinic $C_m^2$ structure for $T \leq 480$ K; c) a and c parameters of the hexagonal $R\bar{3}m$ structure for $T \geq 500$ K.

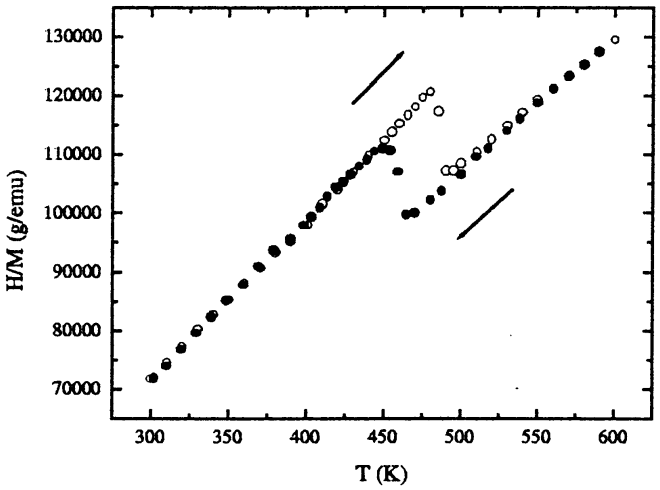


**Fig. 5.** Temperature dependence of $H/M$ at $H = 2$ T for $NaNiO_2$ showing hysteresis around the JT transition.

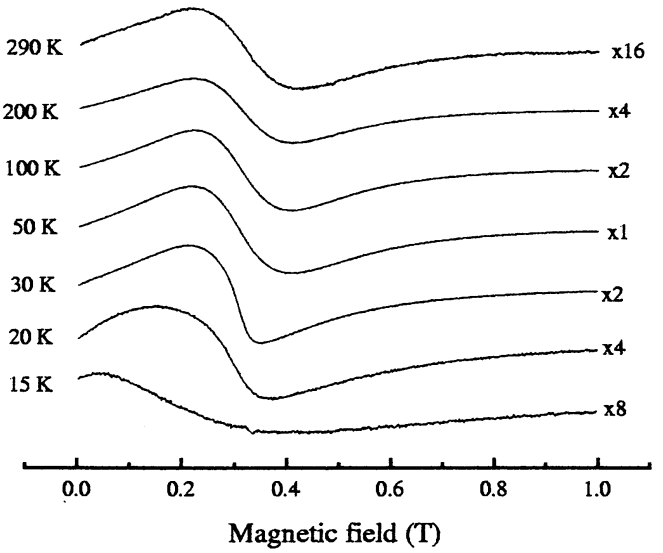


**Fig. 6.** ESR spectra of $NaNiO_2$ taken at 9.44 GHz for different temperatures.

the points also follow a Curie-Weiss law but with different parameters $\mu_{\text{eff}} = 2.07\mu_{\text{B}}$ and $\theta = +15$ K. It is clear that the $Ni^{3+}$ ions are in the low spin state ($t_{2g}^6 e_g^1$) with $S = 1/2$ in the whole temperature range. These results will be discussed in Section 4.

### 3.3 ESR measurements

Figure 6 shows the low frequency ESR spectra of $NaNiO_2$ for different temperatures. In the paramagnetic regime the EPR signal is slightly asymmetric, with a factor $g_{\text{eff}} \cong 2.14$ at 300 K, and very broad. The signal narrows with decreasing temperature while just above the Néel temperature $T_{\text{N}}$ it becomes again very broad and asymmetric (Fig. 7a), while the resonance field drastically decreases (see Fig. 7b). The inverse of the intensity shown

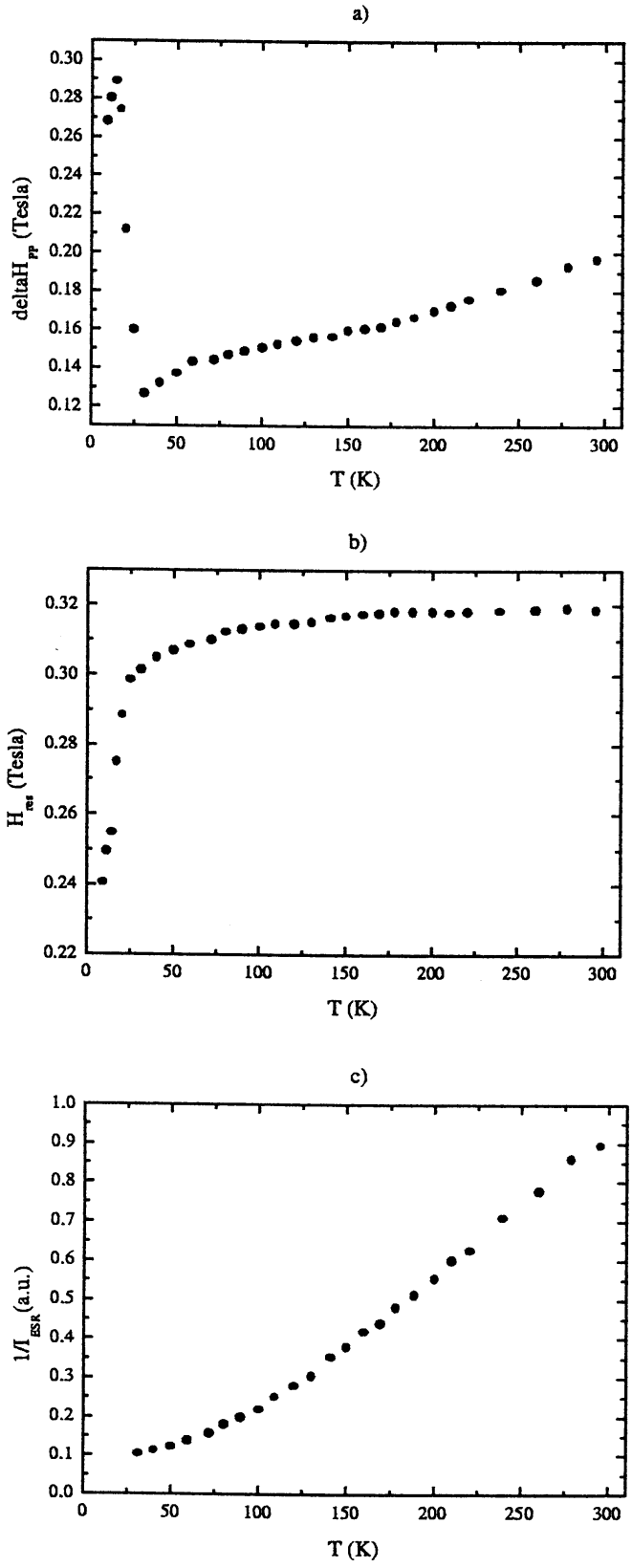


**Fig. 7.** Temperature dependence of a) the linewidth delta$H_{\rm PP}$ b) the resonance field $H_{\rm res}$, and c) the inverse of the ESR intensity for $NaNiO_2$ at 9.44 GHz.

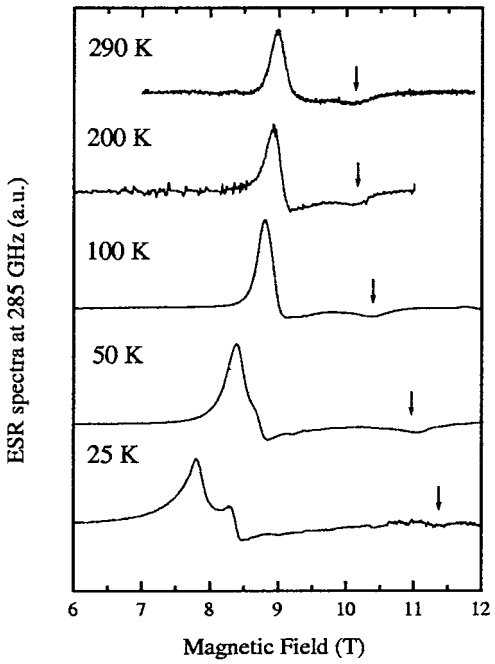


**Fig. 8.** ESR spectra of $NaNiO_2$ taken at 285 GHz for different temperatures.

in Figure 7c is qualitatively similar to the $H/M$ *vs.* $T$ curve for $NaNiO_2$ reported in reference [8]. It is interesting to note that the EPR spectrum of $NaNiO_2$ shown here is similar to the spectra observed for $Li_{1-x}Ni_{1+x}O_2$ with very low $x$ ($x \leq 0.01$) [10]. The linear temperature decrease of the linewidth in $NaNiO_2$ can be attributed to a phonon modulation of the exchange and dipole-dipole interactions rather than to a temperature dependence of the exchange integral [11]. The close packing of the $Ni^{3+}$ ions in the Ni layers will favour this effect. The same linewidth linear temperature dependence has been observed in both, $Li_{1-x}(Ni,Co)_{1+x}O_2$ and $Li_{1-x}Ni_{1+x}O_2$ [11–13]. Azzoni *et al.* [13] proposed a signal-narrowing mechanism associated with the lowering of the hopping frequency of the hole shared by the Ni ions, when the temperature decreases. However, the absence of additional holes in stoichiometric $NaNiO_2$ suggests that this mechanism is not relevant for this family of compounds.

Figures 8 and 9 show our ESR study between 25 and 290 K at 285 GHz. The ESR spectra look anisotropic and the two lines (the higher field one is indicated by an arrow in Fig. 8) can be analysed using two $g$ factors. The temperature dependence of the resonance fields at 285 GHz is plotted in Figure 9.

Figure 10 presents the ESR spectra at 200 K for three selected frequencies. It clearly shows the interest of high frequency measurements: at 115 GHz the two lines mix while at 285 GHz they are well separated. Taking this data into account we plot the frequency-field diagram of Figure 11, from which we derive: $g_{\|} = 2.030$ and $g_{\perp} = 2.283$.

One finds $g_{\|} < g_{\perp}$ as expected for a $Ni^{3+}$ ion in an elongated octahedral environment [15]. The mean $g$ value

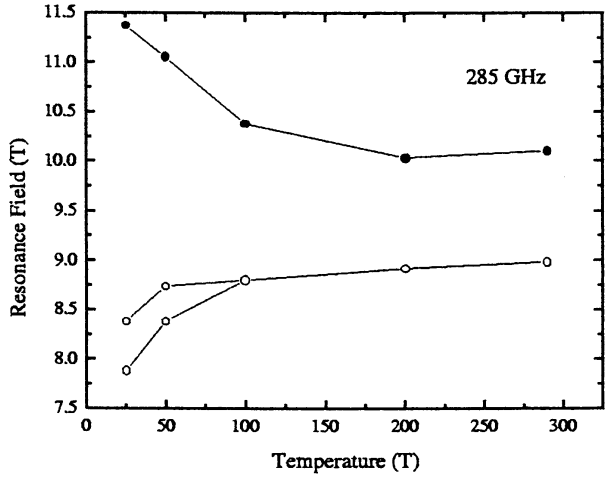


**Fig. 9.** Temperature dependence of the resonance fields for the same frequency of Figure 8.

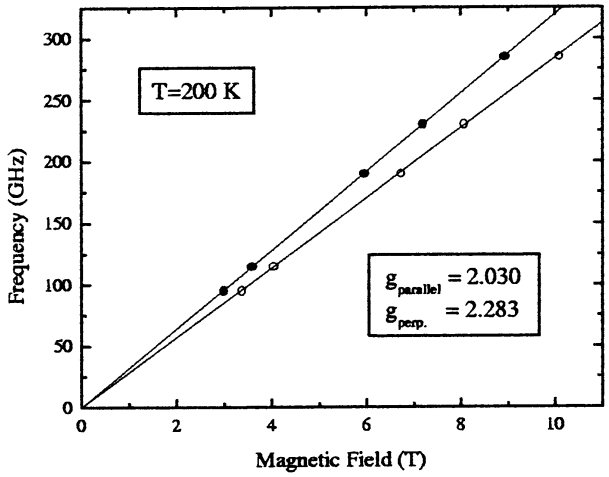


**Fig. 11.** Frequency-field diagram of $NaNiO_2$ derived from Figure 10.

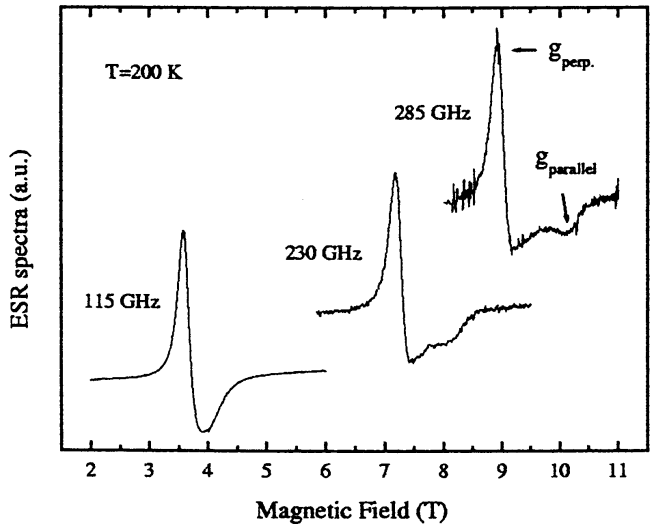


**Fig. 10.** Selected ESR spectra of $NaNiO_2$ below the JT transition at various frequencies.

does not change significantly above 50 K as observed in X-band ESR but the splitting of the resonance starts at 100 K. Deviation from the paramagnetic linear regime of the susceptibility has been already observed well above the Néel temperature $T_N = 20$ K [8]. These effects are signatures of short range ferromagnetic interactions in the Ni layers: $NaNiO_2$ is in fact a quasi-2D system since the magnetic Ni layers are well isolated by the diamagnetic Na layers. The splitting and the new line observed below 100 K have certainly a magnetic origin since they are frequency dependent.

## 4 Discussion

The strong crystal field stabilises the low configuration $^2\Gamma_3$ state ($t_{2g}^6 e_g^1$) as the ground state of the $Ni^{3+}$ ions. The Hund's rule ground state $^4\Gamma_4$ state ($t_{2g}^5 e_g^2$) is the first excited state. The only degeneracy permitted in the ground state of a quantum system is the Kramers degeneracy connected with the invariance with respect to time inversion. Indeed the orbital degeneracy is lifted by a deformation which reduces the symmetry: this is the Jahn-Teller effect [15]. $NaNiO_2$ experiences a CJTE or orbital ordering around 480 K. We have seen that neutron diffraction data refinements at room temperature indicate that there are 4 short and 2 long Ni-O distances. The elongation of the $O$ octahedron decreases the Coulomb energy of the $|\ 3z^2-r^2\rangle$ orbital compared to the $|\ x^2-y^2\rangle$ state, hence the former is the ground state for every $Ni^{3+}$ ion. The axial field also splits the $^2\Gamma_3$ state into two Kramers doublets of configuration $t_{2g}^6 e_g^1 = \overline{e_g^3}$. The spin-orbit coupling connects the ground state to the levels with $t_{2g}^5 e_g^2 = \overline{e_g^2 t_{2g}^1}$ configuration, and gives rise to a residual orbital momentum.

A $g$ value calculation can be made using strong field and single electron wave functions [14]. Equations (1) give the $g$-values expected for the wave functions $U \sim|\ 3z^2-r^2\rangle$ and $V \sim|\ x^2-y^2\rangle$ of the ground state doublet:

$$\begin{cases} g_\parallel(V) = g_e + \frac{4\zeta}{\epsilon} + \Delta \\ g_\perp(V) = g_e + \frac{\zeta}{\epsilon} + \Delta \\ g_\parallel(U) = g_e + \Delta \\ g_\perp(U) = g_e + \frac{3\zeta}{\epsilon} + \Delta \end{cases} \quad (1)$$

where $g_e = 2.0023$ is the Landé factor, $\zeta$ is the spin-orbit constant, $\epsilon$ is a function of the energy of the excited levels ($t_{2g}^5 e_g^2$) configuration reported in the $d^7$ Tanabe and Sugano diagram [16], and $\Delta = 2[\zeta/E(^4\Gamma_4)]^2$, in which $E(^4\Gamma_4)$ is the crystal-field splitting between the ground state $^2\Gamma_3$ and the excited state $^4\Gamma_4$. We do not know this last quantity but since the $\Delta$ term adds in all equations in (1) it does not change the hierarchy. The eigenvalues of the $g$ tensor of the ESR signal shown in Figure 10 ($g_\perp > g_\parallel$) indicate that $U \sim|\ 3z^2-r^2\rangle$ is the occupied state, in agreement with the neutron diffraction data.

The effective moment is lower below the CJTE transition and gets closer to the value expected for $g = 2$ and $S = 1/2$ ($\mu_{\rm eff} = 1.73\mu_{\rm B}$). The orbital momentum is quenched at all temperatures but the spin-orbit coupling tends to create a residual momentum by connecting the ground state with the $^4\Gamma_4$ excited levels. Since the JT effect changes the splitting between these levels it can induce the observed lowering of the effective momentum (see Sect. 3.2).

The positive $\theta$ values derived above from the magnetic susceptibility indicate that the intraplane ferromagnetic interactions are dominant. The increase of $\theta$ below the JT transition can be understood by the distortion of the $NiO_6$ octahedra, since superexchange $Ni^{3+}$-O-$Ni^{3+}$ interactions are very sensitive to the bond angle and distances, that become smaller (see Tab. 3), favouring ferromagnetism.

We have proposed that $NaNiO_2$ could be a model for pure $LiNiO_2$ [3], the presence of additional Ni ions in the Li layers giving rise to the formation of ferromagnetic clusters that inhibits the antiferromagnetic empilement of the ferromagnetic Ni layers in the non-stoichiometric compounds. However, the non observation of a CJTE at lower temperature for $Li_{1-x}Ni_{1+x}O_2$ has been a mystery since its first synthesis by Goodenough *et al.* in 1958 [18]. And in order to explain this as well as the absence of magnetic order, an orbital-liquid spin picture has been recently suggested for $Li_{1-x}Ni_{1+x}O_2$, invoking that the more 3D nature of this compound will favour fluctuations between different classical ordered configurations [1]. Another proposal is that simply the triangular Ni lattice prevents a staggered orbital ordering for the degenerate $e_g$ states, inducing different sign interactions [2]. These two proposals argue that the orbital degeneracy is lifted by the Hund's rule exchange and not by the JT effect. It is quite surprising that authors do not compare this system with isomorphic $NaNiO_2$ in which the triangular lattice does not induce any orbital or spin frustrations (since both have ferromagnetic character). Furthermore, an EXAFS study [19] done for quasi-stoichiometric $Li_{1-x}Ni_{1+x}O_2$ showed the existence of two different Ni-O bond lengths: 4 bonds of 1.91 Å and 2 bonds of 2.09 Å. This elongation of the $NiO_6$ octahedra occurs even at room temperature and results from the JT effect of the $Ni^{3+}$ ions as in $NaNiO_2$. This seems to indicate that the JT effect is the relevant process for the breakdown of orbital degeneracy. However, for $Li_{1-x}Ni_{1+x}O_2$ the JT effect remains local. Armstrong *et al.* noticed that the replacement of $Mn^{3+}$ by $Co^{3+}$ in $LiMnO_2$ results in a shortening of the (Mn/Co)-O bond, approaching the Ni-O bond length in $Li_{1-x}Ni_{1+x}O_2$. They propose that the absence of CJTE in $Li_xMn_{1-y}Co_yO_2$ and in $Li_{1-x}Ni_{1+x}O_2$ may have a similar origin, keeping in mind that very small transition metal vacancies are able to destroy the orbital ordering [20].

## 5 Conclusions

In a recent paper we have shown that at low temperatures $NaNiO_2$ is an A-type antiferromagnet, with a ferromagnetic coupling $J_{\rm F} = +13$ K between the $Ni^{3+}$ ions in the same layer and an antiferromagnetic interaction $J_{\rm AF} = -1$ K between $Ni^{3+}$ ions in adjacent Ni layers [8]. The Néel temperature is 20 K.

Here we have performed a detailed analysis of the CJTE for $NaNiO_2$ and completed the study of this system at high temperatures. We summarise now the results.

This system undergoes a structural transition from a high temperature rhombohedral phase to a low temperature monoclinic phase. We have shown that the transition has a width of approximately 20 K in which the two phases coexist, and its mean value is shifted by cooling or heating the samples. The orbital degeneracy of the $e_g$ levels is lifted by the cooperative Jahn-Teller effect, the elongation of the octahedral environment of the $Ni^{3+}$ ions favouring the occupation of the $|\, 3z^2 - r^2\rangle$ orbital state. Therefore, the triangular Ni lattice has ferrodistorsive orbital ordering in $NaNiO_2$.

From the magnetic susceptibility above the JT transition, we can derive, using a molecular field approach, a ferromagnetic coupling $J_{\rm F} \approx \theta/3 - J_{\rm AF} \approx +6$ K within the Ni layers. Considering a small increase of $J_{\rm AF}$ due to decrease of the interplane distance, this $J_{\rm F}$ value will become even closer to $J_{\rm F} = +8$ K found in quasi-stoichiometric $Li_{1-x}Ni_{1+x}O_2$ ($x \leq 0.01$) [3,10,17]. This is not really surprising since $Li_{1-x}Ni_{1+x}O_2$ and the high temperature phase of $NaNiO_2$ have the same symmetry ($R\bar{3}m$).

Our proposal of $NaNiO_2$ as a model for stoichiometric $LiNiO_2$ [3] seems to be also supported by the striking resemblance of the EPR spectra shown here with those of reference [10].

The absence of a CJTE in $Li_{1-x}Ni_{1+x}O_2$ is still disturbing, however the same type of distortion but with local character has been observed [19]. Experiments on $NaNiO_2$ under pressure will be another test for the different theories quoted in the discussion.

We are indebted to R. Buder from the Laboratoire d'Études des Propriétés Électroniques des Solides (CNRS, Grenoble, France) for the X-band EPR measurements, and to Ph. Lethuiller and E. Eyraud from the Laboratoire Louis Néel (CNRS, Grenoble, France) for the magnetic susceptibility measurements at high temperature. The French CRG-CNRS group at ILL is acknowledged for making available the beam time. This work is a partial fulfillment of the Ph.D. thesis of E. Chappel.

## References

1. L.F. Feiner, A.M. Oles, J. Zaanen, Phys. Rev. Lett. **78**, 2799 (1997); Phys. Rev. B **61**, 6257 (2000).
2. K. Yamaura, M. Takano, H. Hirano, R. Kanno, J. Solid State Chem. **127**, 109 (1996); Y. Kitaoka *et al.*, J. Phys. Soc. Jpn **67**, 3703 (1998).
3. M.D. Núñez-Regueiro, E. Chappel, G. Chouteau, C. Delmas, Eur. Phys. J. B **16**, 37 (2000).

4. L.D. Dyer, B.S. Borie, G.P. Smith, J. Am. Chem. Soc. **76**, 1499 (1954).
5. P.F. Bongers, U. Enz, Solid State Comm. **4**, 153 (1966).
6. S. Dick, M. Müller, F. Preissinger, T. Zeiske, Powder Diffraction **12**, 239 (1997).
7. C. Delmas, I. Saadoune, P. Dordor, Mol. Cryst. Liq. Cryst. **244**, 337 (1994).
8. E. Chappel, M.D. Núñez-Regueiro, F. Dupont, G. Chouteau, C. Darie, A. Sulpice, Eur. Phys. J. B **17**, 609 (2000).
9. J. Rodriguez-Carvajal, Phys. B **192**, 55 (1993).
10. V. Bianchi, E. Chappel, D. Caurant, N. Baffier, C. Belhomme, S. Bach, J.P. Pereira Ramos, G. Chouteau, A. Sulpice, P. Willmann (in press).
11. R. Stoyanova, E. Zhecheva, C. Friebel, J. Phys. Chem. Solids **54**, 9 (1993).
12. R. Stoyanova, E. Zhecheva, C. Friebel, Solid State Ionics **73**, 1 (1994).
13. C.B. Azzoni, A. Paleari, V. Massarotti, D. Capsoni, J. Phys. Cond. Matt. **8**, 7339 (1996).
14. R. Lacroix, U. Höchli, K.A. Müller, Helv. Phys. Acta **37**, 627 (1964).
15. H.A. Jahn, E. Teller, Proc. R. Soc. London, Ser. A **161**, 220 (1937).
16. S. Sugano, Y. Tanabe, H. Kamimura, *Multiplets of transition-metal ions in crystals* (Academic Press, New York and London, 1970).
17. M.D. Núñez-Regueiro, E. Chappel, G. Chouteau, C. Delmas, Mol. Cryst. Liq. Cryst. **177**, 341 (2000).
18. J.B. Goodenough, D.G. Wickham, W.J. Croft, J. Phys. Chem. Solids **5**, 107 (1958).
19. A. Rougier, C. Delmas, A.V. Chadwick, Solid State Comm. **94**, 123 (1995).
20. A.R. Armstrong, A.D. Robertson, R. Gitzendanner, P.G. Bruce, J. Solid State Chem. **145**, 549 (1999).